ILASS 2008
Sep. 8-10, 2008, Como Lake, Italy

Paper ID ILASS08-2-4

ENHANCEMENT AND VALIDATION OF AN EULERIAN-EULERIAN APPROACH FOR DIESEL SPRAYS

Milan Vujanović*, Wilfried Edelbauer°, Eberhard von Berg°,
Reinhard Tatschl° and Neven Duić*

* Faculty of Mechanical Engineering and Naval Architecture, University of Zagreb, Zagreb, Croatia
° AVL List GmbH, Graz, Austria

ABSTRACT

Turbulent sprays in computational fluid dynamics calculations (CFD) of internal combustion engines are usually modelled based on the most commonly used Eulerian-Lagrangian method, also known as the Discrete Droplet Model (DDM). This method is especially suitable for the modelling of dilute sprays, but has some disadvantages near nozzle region with respect to insufficient description of the physics in a dense spray, where the bulk liquid phase disintegrates into droplets. This can be improved by stronger physical coupling of the gas and the liquid phase in the near nozzle region using an Eulerian-Eulerian multiphase method. This method provides a more accurate description of the physics in the dense spray region by treating each droplet size class as completely separate phase and solving conservation equations for each of them. The focus of this paper is therefore on the application and validation of the Eulerian-Eulerian spray model. In the standard approach the model deals with fixed droplet size classes, while in an advanced model approach variable size classes are applied. The work presented below on diesel sprays establishes a validated modelling concept that can be applied with confidence for accurate calculation of the dense liquid spray. Several simulations of high pressures diesel injections have been carried out, using AVL's CFD code FIRE, and compared with experimental data.

INTRODUCTION

Pollutant emissions from diesel engines have been regulated for several decades, and new and more stringent regulations are expected within this decade. In response to these regulations, the increase of fuel efficiency continues to be a major challenge in modern engineering development process. The performance and fuel efficiency of diesel engines highly depends on the injector atomizer system and resulting spray behaviour, particularly on the quality of fuel-air mixture, which is a key to maximizing fuel efficiency, and minimizing pollutant emissions of the engine. Therefore, an appropriate computer modelling of liquid-fuel spray dynamics is essential to provide insight and understanding of the spray flows in diesel engines.

Different modelling approaches currently exist for multiphase droplet flows as Eulerian-Lagrangian, Eulerian-Eulerian Multiphase, Volume of Fluid (VOF) etc.

The Lagrangian-Eulerian approach has been used by many researchers and various improvements to the basic scheme have been proposed [1], [2], [3], [4], and [5]. In recent years this approach has dominated for predicting the behaviour of spray. Although various researchers and engineers have used Lagrangian-Eulerian formulation as a numerical simulation tool for prediction of characteristic of complex multiphase droplet flows to guide their engineering devices design, the concept and application have severe limitations. This formulation is very sensitive to the grid resolution in the near nozzle region [6], [7] and it reveals limitations in the description of dense sprays. This assumes that spray is sufficiently diluted; usually discrete phase volume fraction must be less than 10 %. It also shows statistical convergence problems as discussed by [8] and [9]. This can be improved by stronger physical coupling of the gaseous and the liquid phases using the Eulerian-Eulerian multiphase method, where a cloud of droplets is regarded as continuum and conservation equations are solved for gas and liquid phase. This means that the Eulerian description is applied to the dispersed liquid phases, which can be treated with the same discretization, similar numerical techniques and governing equations as used for the gaseous phase. This approach was firstly addressed by Harlow and Amsden [10], [11]. The Eulerian-Eulerian approach has been adopted by a number of researches and applied for numerical simulation, e.g. [12], [13], [14], [15], and [16]. Compared to the Lagrangian scheme, the Eulerian scheme calculation is fairly efficient for flows of high droplet concentration, while the Lagrangian scheme, particularly for unsteady calculations, generally requires a large number of parcels in each control volume of the calculation domain. However, in order to better capture the behaviour of spray and characteristic of droplets in dense region using the Eulerian framework, the droplet-size distribution has to be divided into a number of separate size classes (n liquid phases), where each phase requiring its own set of conservation equations.

The focus of this work is on application, optimisation and validation of the Eulerian-Eulerian spray modelling concept in high pressure dense diesel sprays. The numerical simulations of the sprays performed in this work have been based on the Eulerian-Eulerian approach, which was integrated into the commercial AVL CFD code FIRE. The validation of the Eulerian-Eulerian spray model against experimental data representing one of the basic requirements for the accurate prediction of spray flows has been used for further improvement and development of the physical spray models in the CFD code FIRE. Several simulations of high pressures diesel injections combined with different chamber pressure, using a standard approach with fixed droplet size

classes, have been carried out and compared with experimental data. In addition, the standard Eulerian approach has been extended by variable droplet size classes representing the advanced model approach, and simulation results for one operating point are presented.

EULERIAN SPRAY MODEL

Standard approach with fixed droplet size classes

The basis of the Eulerian spray model is the multi-phase approach obtained through the ensemble averaging process of the conservation equations [17]. The different phases, here gas and liquid, are treated as interpenetrating continua represented by their phase volume fractions. Furthermore, the liquid is divided into different droplet size classes; each represented by a separate droplet phase. Table 1 shows the phase specification of the model. The first phase is always the gaseous phase for the gas mixture. The vapor mass fraction is transported by a separate scalar transport equation within the gaseous phase. The next phases from 2 to *n*-1 are the liquid droplet phases. In the standard Eulerian spray model a constant droplet class diameter is assigned to each of these phases. In the advanced Eulerian spray approach the droplet size class diameter is variable. The last phase *n* of Table 1 is the bulk liquid phase leaving the nozzle and disintegrating into the droplet phases, since primary break-up processes occur. For every phase the complete set of conservation equations is solved. The higher the total number of phases, the higher the resolution in the droplet diameter space, but the higher is also the computational effort.

Table 1: The phase specification of the Eulerian spray model

Phase	1	2, …, n-1	n
Content	Gas mixture	Droplets	Bulk liquid

The multi-phase conservation equations of [17] for mass, momentum, and enthalpy for phase *k* are shown in Eqs. (1), (3) and (4). The compatibility condition Eq. (2) for the phase volume fractions α_k must be satisfied. The right hand sides of the conservation equation contain the exchange terms between the phases, Γ_{kl}, $\mathbf{M}_{kl}$ and H_{kl}. These terms contain the appropriate physics of the spray model, while the left hand sides determine the rate of change and convective transport of the flow properties of the phases.

$$\frac{\partial \alpha_k \rho_k}{\partial t} + \nabla \cdot \alpha_k \rho_k \mathbf{v}_k = \sum_{l=1,l\neq k}^{n} \Gamma_{kl} \tag{1}$$

$$\sum_{k=1}^{n} \alpha_k = 1 \tag{2}$$

$$\frac{\partial \alpha_k \rho_k \mathbf{v}_k}{\partial t} + \nabla \cdot \alpha_k \rho_k \mathbf{v}_k \mathbf{v}_k = -\alpha_k \nabla p + \nabla \cdot \alpha_k (\boldsymbol{\tau}_k + \boldsymbol{\tau}_k^t) + \alpha_k \rho_k \mathbf{f} + \sum_{l=1,l\neq k}^{n} \mathbf{M}_{kl} + \mathbf{v}_k \sum_{l=1,l\neq k}^{n} \Gamma_{kl} \tag{3}$$

$$\frac{\partial \alpha_k \rho_k h_k}{\partial t} + \nabla \cdot \alpha_k \rho_k \mathbf{v}_k h_k = \nabla \cdot \alpha_k \left(\mathbf{q}_k + \mathbf{q}_k^t\right) + \alpha_k \rho_k \mathbf{f} \cdot \mathbf{v}_k + \alpha_k \rho_k \theta_k + \alpha_k \boldsymbol{\tau}_k : \nabla \mathbf{v}_k + \alpha_k \frac{dp}{dt} + \sum_{l=1,l\neq k}^{n} \mathrm{H}_{kl} + h_k \sum_{l=1,l\neq k}^{n} \Gamma_{kl} \tag{4}$$

The turbulence is modelled with the standard *k*-ε model, where the equation

$$\frac{\partial \alpha_k \rho_k k_k}{\partial t} + \nabla \cdot \alpha_k \rho_k \mathbf{v}_k k_k = \nabla \cdot \alpha_k \left(\mu_k + \frac{\mu_k^t}{\sigma_k} \right) \nabla k_k + \alpha_k \boldsymbol{\tau}_k^t : \nabla \mathbf{v}_k - \alpha_k \rho_k \varepsilon_k + k_k \sum_{l=1,l\neq k}^{n} \Gamma_{kl} \quad , \tag{5}$$

describes the transport of the turbulent kinetic energy k_k for phase *k*. The turbulent viscosity μ_k^t is modelled by $C_\mu \rho_k k_k^2/\varepsilon_k$, where the turbulence dissipation rate ε_k of phase *k* is obtained from the following transport equation

$$\frac{\partial \alpha_k \rho_k \varepsilon_k}{\partial t} + \nabla \cdot \alpha_k \rho_k \mathbf{v}_k \varepsilon_k = \nabla \cdot \alpha_k \left(\mu_k + \frac{\mu_k^t}{\sigma_\varepsilon} \right) \nabla \varepsilon_k + \varepsilon_k \sum_{l=1,l\neq k}^{n} \Gamma_{kl} + \alpha_k C_1 \left(\boldsymbol{\tau}_k^t : \nabla \mathbf{v}_k \right) \frac{\varepsilon_k}{k_k} - \alpha_k C_2 \rho_k \frac{\varepsilon_k^2}{k_k} - \alpha_k C_4 \rho_k \varepsilon_k \nabla \cdot \mathbf{v}_k \quad . \tag{6}$$

The closure coefficients applied for the *k*-ε turbulence model in Eq. (5) and Eq. (6) are summarised Table 2.

Table 2: Closure Coefficients in the k-ε Model

σ_k	σ_ε	C_1	C_2	C_4	C_μ
1.0	1.3	1.44	1.92	-0.33	0.09

For the vapor mass fraction Y_i an additional transport equation, described by the equation

$$\frac{\partial}{\partial t} \alpha_1 \rho_1 Y_i + \nabla \cdot \alpha_1 \rho_1 \mathbf{v}_1 Y_i = \nabla \cdot \left(\alpha_1 (\rho_1 \mathrm{D}_{Y_i} + \frac{\mu_1^{\mathrm{t}}}{\mathrm{Sc}^t}) \nabla Y_i \right) + S_{Y_i} \quad , \tag{7}$$

is solved for the gaseous phase 1. The source term S_{Yi} is determined by the sum of the evaporated liquid masses of all droplet phases from 2 to *n*.

The interfacial mass exchange term Γ_{kl} in Eq. (1) describes the mass exchange between the phases *k* and *l*. It gets its contributions from droplet evaporation *E*, primary break-up *P* and secondary break-up *S*, as described by

$$\Gamma_{kl} = \Gamma_{E,kl} + \Gamma_{P,kl} + \Gamma_{S,kl} \quad . \tag{8}$$

The mass exchange between two phases for a process acts in both directions, so that one can write $\Gamma_{Process,kl} = -\Gamma_{Process,lk}$. This means that a mass gain for phase *k* is a mass loss for phase *l* and vice versa, so that mass conservation over all phases is ensured. Evaporation takes place between the liquid

phases from 2 to n and the gaseous phase 1. The interfacial mass exchange rate due to evaporation between the droplet phase k and the gaseous phase 1 is determined by the equation

$$\Gamma_{E,k1} = -N_k \dot{m}_{E,k1} = -\Gamma_{E,1k} \quad , \tag{9}$$

where droplet number density N_k denotes the number of droplets per unit volume. Assuming spherical droplets with diameter D_k, N_k can be derived from the equation

$$\frac{\pi D_k^3}{6} N_k = \alpha_k \rightarrow N_k = \frac{6\alpha_k}{\pi D_k^3} \quad . \tag{10}$$

The term $\dot{m}_{E,kl}$ determines the evaporated mass exchange rate of a single droplet calculated according to the model of Abramzon & Sirignano [18]. The negative sign in Eq. (9) results from the sign convention of the evaporation model in [18], where evaporated mass being a mass loss for the considered phase, has positive sign.

Figure 1 shows the break-up behavior in the Eulerian spray model. The droplet classes are sorted in ascending manner, where phase 2 denotes the droplet phase with the smallest size class diameter. The bulk liquid phase n disintegrates into the droplet phases from 2 to n-1. The droplets produced from primary break-up are subject to further secondary break-up processes, where every droplet phase k may disintegrate into droplets with smaller size class diameter from 2 to k-1.

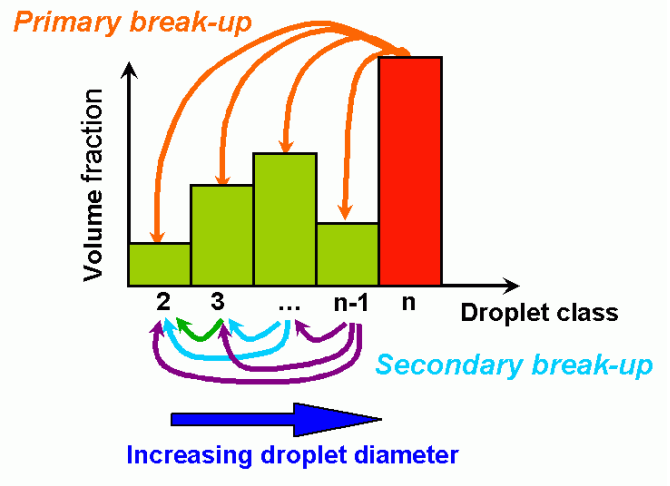

Figure 1: *Mass exchange in the Eulerian spray model due to primary and secondary break-up*

Blob injection with decreasing number of blobs, as described in Figure 2 a), is assumed for the standard Eulerian spray model. This means that the mass loss of the parent droplet class resulting in a reduction of the phase volume fraction α_k leads to reduction of the number of blobs N_k, since the size class diameter D_k stays constant.

The mass exchange rate due to primary and secondary break-up, $\Gamma_{P,nl}$ and $\Gamma_{S,kl}$, are determined by the diameter change rates $(dD_n/dt)_{P,nl}$ and $(dD_k/dt)_{S,kl}$ of the disintegrating blobs. The equation

$$\Gamma_{Br,nl} = \frac{1}{2} N_n \rho_n \pi D_n^2 \left(\frac{dD_n}{dt} \right)_{Br,nl} = \frac{3\alpha_n \rho_n}{D_n} \left(\frac{dD_n}{dt} \right)_{Br,nl} = -\Gamma_{Br,ln} \quad , \tag{11}$$

denotes the general break-up mass exchange rate, where index Br has to be replaced with P for primary and with S for secondary break-up. The disintegration rate of the bulk liquid phase n into the droplet phase l, $(dD_n/dt)_{P,nl}$, is calculated with the model of Bianchi & Pelloni [19] considering two independent mechanisms, aerodynamic surface wave growth and internal stresses by injector flow turbulence. The diameter change rate of the blob due to secondary break-up $(dD_k/dt)_{S,kl}$ is modelled by the standard WAVE model [20]. The break-up models are applied in each cell of the spray region. If the predicted size of break-up products D_l is less than the parent drop diameter D_k, mass is transferred according to the break-up rate into the corresponding droplet size class. The break-up model equations for both, primary and secondary break-up, as well as the translation of the equation into the Eulerian frame are described in more detail in [21], [22], [23] and [24].

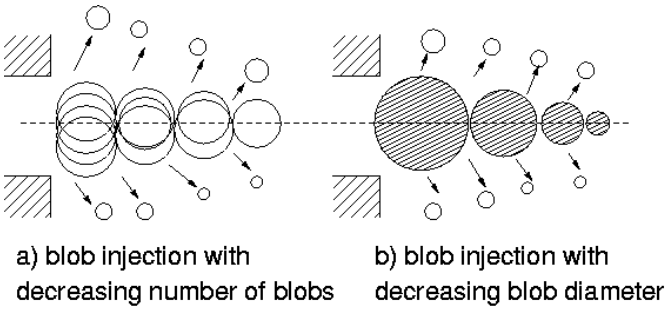

Figure 2: *Numerical approaches for primary break-up*

The momentum exchange between the gaseous phase 1 and the liquid phases k from 2 to n, $\mathbf{M}_{k1}$, is determined by drag forces, $\mathbf{M}_{D,k1}$, and turbulent dispersion forces, $\mathbf{M}_{T,k1}$, as shown by the equation

$$\mathbf{M}_{k1} = \mathbf{M}_{D,k1} + \mathbf{M}_{T,k1} = = c_D \frac{6\alpha_k \rho_1}{D_k} |\mathbf{v}_1 - \mathbf{v}_k| (\mathbf{v}_1 - \mathbf{v}_k) + c_T \rho_1 k_1 \nabla \alpha_k = -\mathbf{M}_{1k} \quad . \tag{12}$$

The drag coefficient c_D is a function of the droplet Reynolds number, the liquid volume fraction and the droplet deformation. The turbulent dispersion force is modelled following the approach of [25], with a constant or modelled turbulent dispersion force coefficient c_T.

The evaporation model determines the interfacial enthalpy exchange, H_{k1}, between the gaseous phase and the liquid phases. The term $\dot{Q}_{E,k1}$ in Eq. (13) represents the heat flow rate into a single droplet and is calculated according to the correlation of [18].

$$H_{k1} = N_k \dot{Q}_{E,k1} = \frac{6\alpha_k}{\pi D_k^3} \dot{Q}_{E,k1} = -H_{1k} \tag{13}$$

Advanced approach with variable droplet size classes

The target of the advanced Eulerian spray model was to overcome the limitations of the fixed droplet size classes. Since the evaporation dynamics depends on the droplet diameter, the evaporation with fixed droplet size classes may be underestimated. Thus, by ensuring enough droplets of small size the break-up models have to compensate this effect. As a consequence of this break-up compensation all of the mass might be shifted into the class with the smallest diameter leading to poor resolution of the droplet size distribution. Therefore the model has been extended by using the idea of variable droplet size classes, which allows for improved resolution by using all of the size classes during the temporal evolution of size distribution and by tracking the diameter evolution inside each class. Therefore, Eq. (10) can be rewritten to extract the phase droplet diameter D_k, as described by the equation

$$D_k = \left(\frac{6\alpha_k}{\pi N_k} \right)^{\frac{1}{3}} \quad . \tag{14}$$

Thus, by solving additional transport equations for the droplet phase number densities for every liquid phase k, according to the equation

$$\frac{\partial N_k}{\partial t} + \nabla \cdot (N_k \mathbf{v}_k) = \sum_{k=2}^{n} \Pi_k \quad , \tag{15}$$

the droplet size class diameter can be calculated locally with the number density N_k and the volume fraction α_k. Within the considered droplet size class k there is still one single diameter, however, changing with time. Furthermore also the size class borders are continuously adapted. This method is applied locally in each computational cell favouring an optimum resolution in each region of the domain. The number density source term Π_k gets its contributions from all processes producing or annihilating droplets. Evaporation E and thermal expansion Th due to temperature change lead to a change of the droplet diameter, but do not influence the number of droplets. Thus, $\Pi_{E,k}$ and $\Pi_{Th,k}$ for k from 2 to n are zero. Number density sources from collision and coalescence are not yet considered. Primary and secondary break-up processes generate new droplets, and hence, the number density source term Π_k equals

$$\Pi_k = \Pi_{P,k} + \Pi_{S,k} \quad . \tag{16}$$

For the Eulerian spray model with variable droplet size classes, the primary break-up approach corresponds to the sketch in Figure 2 b) showing blob injection with decreasing blob diameter. The bulk liquid phase has no source, $\Pi_{P,k=n} = 0$, since the child droplets are stripped from the parent droplet without changing their number. The produced child droplets of phase k generate the number density source according to the equation

$$\Pi_{P,k} = -\frac{6\,\Gamma_{P,nk}}{\pi\, D_k^3\, \rho_k} \quad \text{for} \quad k = 2,\ldots,n-1 \quad . \tag{17}$$

In the present model secondary break-up occurs, if parent droplets belonging to phase l disintegrate into child droplets belonging to phase k, where the class diameter D_l, has to be bigger than the class diameter of D_k. The number density source $\Pi_{S,k}$ is then determined by the sum of the secondary break-up processes producing mass transfer into phase k, as described by the equation

$$\Pi_{S,k} = \sum_{l=2}^{n-1} -\frac{6\,\Gamma_{S,lk}}{\pi\, D_k^3\, \rho_k} \quad \text{for} \quad D_l > D_k \quad . \tag{18}$$

The evolution of the droplet size class diameter over time depends on the evaporation and the break-up processes. The assumption of classes sorted in ascending manner, as shown in Figure 1 for the standard Eulerian spray model, cannot be ensured. Thus, for the determination of the parent and child droplet phases relevant for the break-up processes, the droplet size classes have to be sorted according to their class diameter D_k.

SIMULATION AND VALIDATION

The numerical simulations of the spray have been based on the Eulerian-Eulerian multiphase model implemented in AVL's CFD code FIRE. Five operating points of high-pressure diesel sprays have been used for the simulation cases. A two dimensional computational mesh with 1 400 cells, extending from 0 to 120 mm in axial direction and from 0 to 25 mm in radial direction, and applied axial symmetry in tangential direction, have been used for the simulations. The mesh has been refined towards the spray inlet and the symmetry axis.

Six phases in total have been used, one gaseous phase, four droplet phases and one bulk liquid phase. The size class diameters are 5, 10, 20 and 40 μm for the droplet phases and the nozzle diameter of 205 μm has been assigned to the bulk liquid phase. A variation of sub-model coefficients has been performed and its impact on predictions has been investigated in order to obtain a final set of sub-model coefficients, which was then applied for all simulations of the experimental operating points.

The Figures 3 to **7** show the comparisons of calculated and measured penetration curves of the liquid and the vapor spray tip for different injection pressures combined with different chamber pressure. The standard approach with fixed droplet size classes was applied in these simulations. Since previous simulations had shown systematic underestimated vapor tip penetrations, the model constant C_2 in the turbulence dissipation rate transport equation (Table 2) was adjusted to the value proposed by [26] of C_2=1.8. The adapted value of C_2 causes less reduction of the turbulence dissipation rate, consequently a higher dissipation level ε and a lower level of the turbulent kinetic energy k, finally leading to a lower turbulent viscosity and a better spreading rate.

At this point it is important to mention that the spray contour in the Eulerian-Eulerian spray description is not as easy to detect as in the Lagrangian DDM. The spray contours are determined by the limiting threshold values for the liquid volume fraction and the vapor mass fraction. Once the limiter values are defined for one reference case showing good agreement with the experimental data, the same values have to be used for all other cases to be comparable. More details about the determination of the limiting threshold values can be found in [23]. The stepwise illustration of the spray tip

penetration curves results from the post-processing and depends on the mesh resolution in the corresponding region.

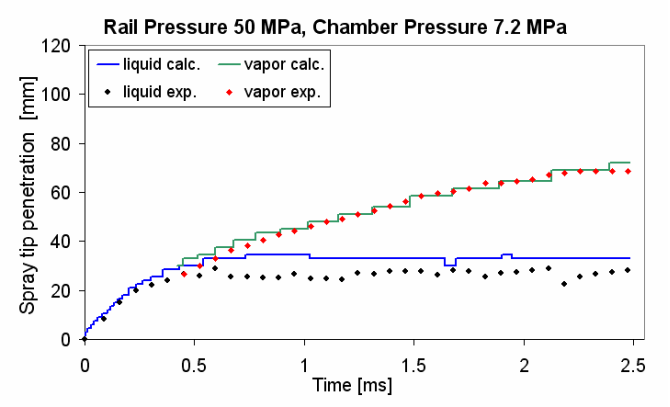

Figure 3: *Comparison of the calculated and measured liquid and vapor penetration at 50 MPa rail pressure and 7.2 MPa chamber pressure*

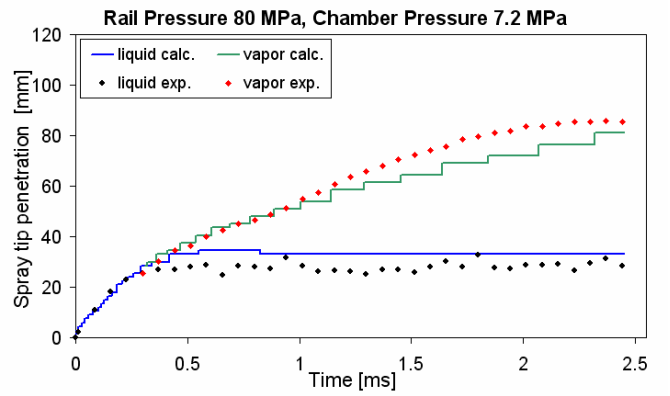

Figure 4: *Comparison of the calculated and measured liquid and vapor penetration at 80 MPa rail pressure and 7.2 MPa chamber pressure*

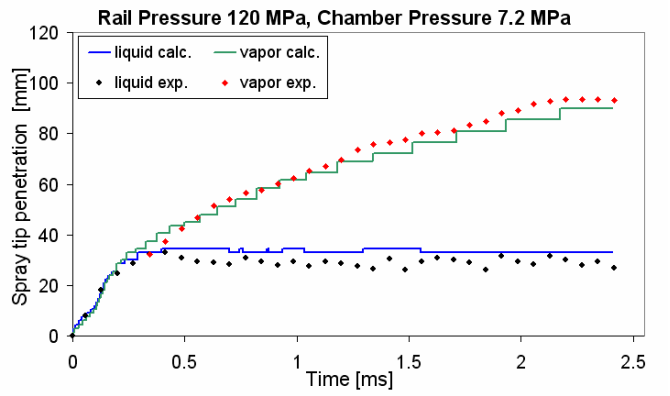

Figure 5: *Comparison of the calculated and measured liquid and vapor penetration at 120 MPa rail pressure and 7.2 MPa chamber pressure*

It can been seen that predicted penetrations for liquid and vapor phase for all simulation cases are in fairly good agreement with the experimental data and that standard Eulerian model with fixed droplet size classes can be taken with confidence for multiphase calculation of dense liquid spray near the nozzle region.

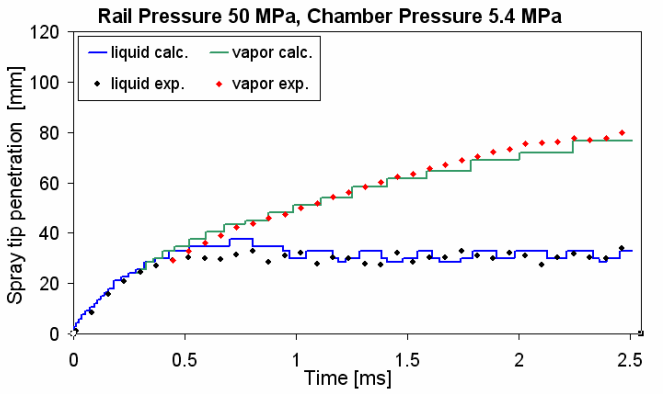

Figure 6: *Comparison of the calculated and measured liquid and vapor penetration at 50 MPa rail pressure and 5.4 MPa chamber pressure*

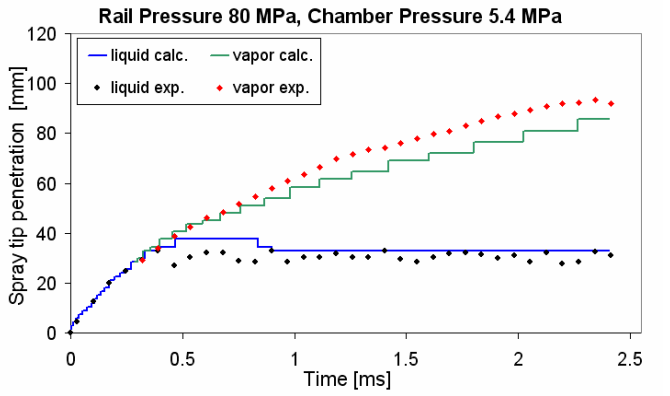

Figure 7: *Comparison of the calculated and measured liquid and vapor penetration at 80 MPa rail pressure and 5.4 MPa chamber pressure*

The advanced model with variable droplet size classes represents an important step forward in the Eulerian spray approach, since it increases the resolution of the droplet size distribution and improves the simulation of the evaporation process. In this paper the simulation results for one case at 120 MPa rail pressure and 7.2 MPa chamber pressure are presented in detail. Figure 8 shows the computational mesh, the total volume fraction, which is the sum over all liquid phase volume fractions, and the vapor mass fraction 2 ms after the start of injection.

As shown in Figure 9 the liquid and the vapor tip penetration calculated with variable droplet size classes are also in good agreement with measurement data.

The local diameters, the phase volume fractions, and the droplet number densities for the droplet phases 2, 3 and the bulk liquid phase 6 are shown in the Figures 11 to 12, 2 ms after start of injection respectively. Due to evaporation the droplet diameters of phase 2 in Figure 10 are continuously decreasing. Figure 11 shows a spot in the number density

field. Since the droplet diameters in the corresponding region do not show a similar spot, one can conclude that this region represents accumulated droplet mass caused by the break-up processes and the droplet transport. As can be seen in Figure 11 the border of the droplet diameter field is different to the total liquid spray contour. Due to numerical reasons every phase has to have a certain minimum value for the volume fraction, and thus, every cell in the computational domain has a certain droplet diameter. For better visualisation, the droplet diameters are plotted only in region of the expected spray contour, which does not necessarily correspond to the real spray contour.

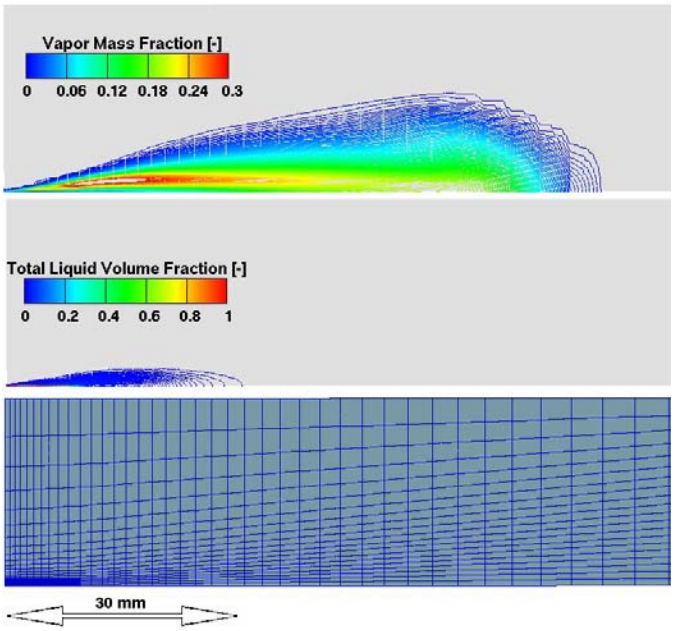

Figure 8: *Total liquid volume fraction and vapor mass fraction 2 ms after start of injection*

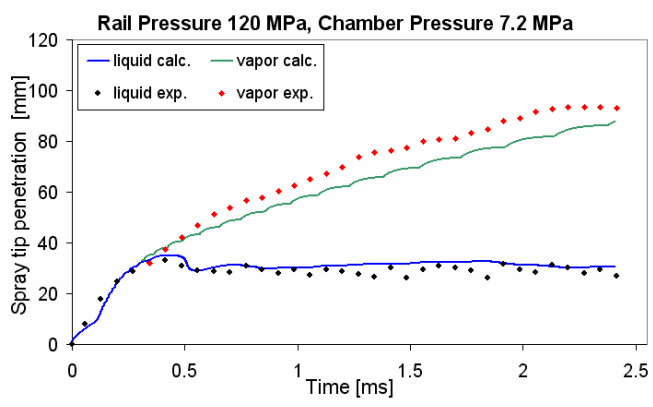

Figure 9: *Comparison of the calculated and measured liquid and vapor penetration at 120 MPa rail pressure and 7.2 MPa chamber pressure by using variable droplet size classes*

It is noticeable as shown in Figure 12 that approximately 1.5 mm away from the orifice the bulk liquid phase 6 is fully disintegrated into the droplet phases. As discussed above, the number density of phase 6 does not change due to primary break-up, since blob injection according to Figure 2 b) is assumed. The mass is shifted to the droplet phases and consequently the droplet diameter decreases.

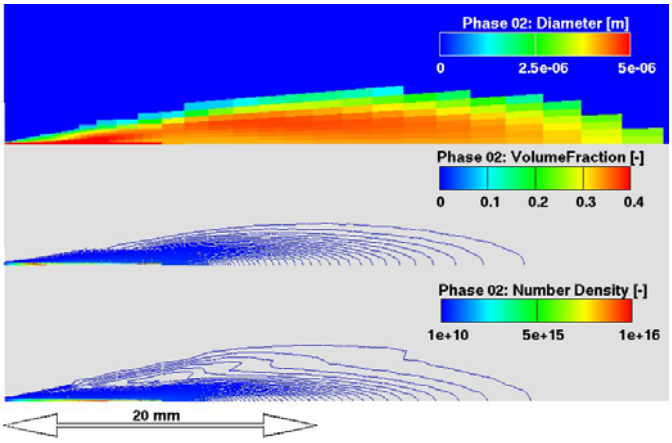

Figure 10: *Local diameter, volume fraction and droplet number density for the liquid phase 2 (2 ms after start of injection)*

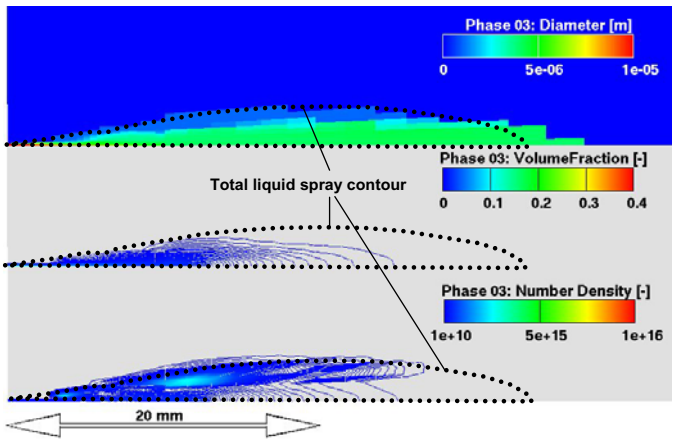

Figure 11: *Local diameter, volume fraction and droplet number density for the liquid phase 3 (2 ms after start of injection)*

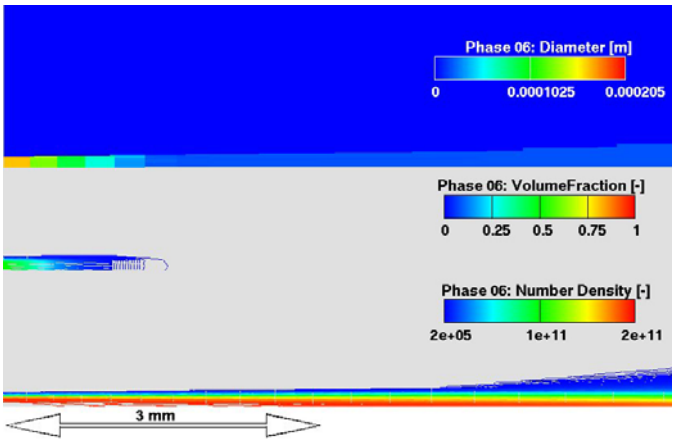

Figure 12: *Local diameter, volume fraction and droplet number density for the liquid phase 6 (2 ms after start of injection)*

Figure 13 shows the total volume fraction, the mean diameters fields for the number mean D_{10}, the volume mean D_{30}, and the Sauter mean D_{32} diameter in the region up to 10 mm away from the nozzle exit. It can be observed that break-up and evaporation processes reduce the droplet diameters. Experimental data for the droplet diameters were not available for comparison.

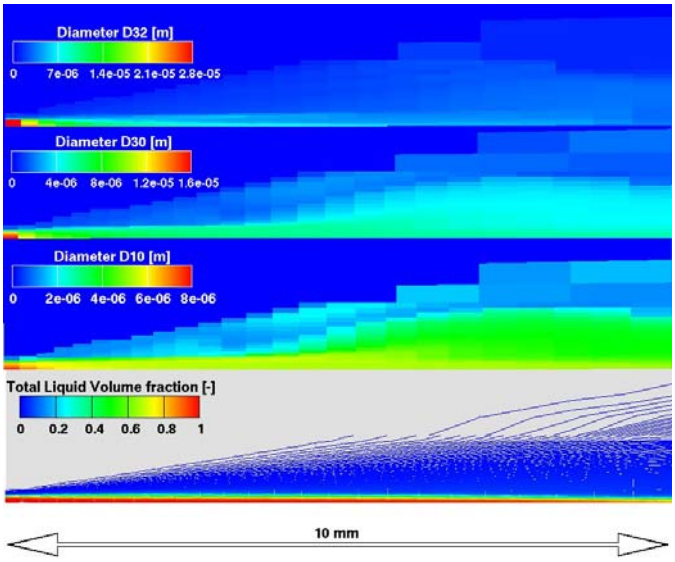

Figure 13: *Total liquid volume fraction and mean diameters D_{10}, D_{30} and D_{32} (2 ms after start of injection)*

CONCLUSION

An Eulerian-Eulerian spray modelling concept, applying the standard approach with constant size class diameters assigned to each of the liquid droplet phases and the advanced approach with the variable droplet size classes, has been presented.

The validation of the standard Eulerian spray model has been achieved by comparing model predictions against experimental data for variation of high-pressure diesel injections at two different chamber pressures. The simulation results are in good agreement with experimental data for liquid and vapor penetration. Consequently, the results confirm that standard Eulerian approach can be applied with confidence for accurate prediction of characteristic of complex multiphase droplet flows in high pressure dense diesel spray simulations.

In addition, the standard validated diesel spray modelling approach has been extended by transporting additional number density transport equations to obtain variable droplet size classes. This approach has been validated for one case for high-pressure diesel injection at 7.2 MPa chamber pressure. The results for liquid and vapor penetration are also in good agreement with experimental data. It is shown that this advanced approach is capable to ensure improved resolution of the droplet size distribution, which is important for improved and accurate prediction of evaporation dynamics.

ACKNOWLEDGEMENTS

This study is partly based on fundings by the European Commission in the framework of the Growth Programme (Project Number: GRD1-1999-10034) and the NICE project (New Integrated Combustion system for future passenger car Engines: TIP3-CT-2004-506201-NICE). The experimental spray data were measured by Dr. Gerhard König at DaimlerChrysler Research Department.

NOMENCLATURE

c, C	Model constant	-
D	Diameter	m
D	Diffusion coefficient of species	m²/s
f	Specific body force vector	m/s²
h	Specific enthalpy	J/kg
H	Enthalpy exchange rate	W/m³
k	Turbulent kinetic energy	m²/s²
M	Momentum exchange rate vector	N/m³
m	Mass	kg
n	Number of phases	-
N	Droplet number density	1/m³
p	Pressure	Pa
q	Heat flux rate	W/m²
Q	Heat transfer	J
S	Species source	kg/s m³
Sc	Schmidt number	-
t	Time	s
v	Velocity vector	m/s
Y	Species mass fraction	-
α	Volume fraction	-
ε	Turbulence dissipation rate	m²/s³
Γ	Mass exchange rate	kg/s m³
μ	Dynamic viscosity	Pa s
θ	Heat source	W/kg
Π	Number density exchange rate	1/s m³
ρ	Density	kg/m³
σ	Model coefficient	-
$\boldsymbol{\tau}$	Stress tensor	N/m²

Subscripts:

Br	Break-up
D	Drag
E	Evaporation
i	Species index
k,l	Phase indices
P	Primary break-up
S	Secondary break-up
T	Turbulent dispersion
Th	Thermal Expansion
Y	Species

Superscripts:

t	turbulent

REFERENCES

[1] J.K. Dukowicz, A Particle-Fluid Numerical Model for Liquid Sprays, *J. Computational Physics 35*, pp. 229-253, 1980.

[2] G. Gouesbet and A. Berlemont, Eulerian and Lagrangian approaches for predicting the behaviour of discrete particles in turbulent flows, *Progress in Energy and Combustion Science*, 25, 2, pp. 133-159, 1998.

[3] E. Loth, Numerical approaches for motion of dispersed particles, droplets and bubbles, *Progress in Energy and Combustion Science*, 26, 3, pp. 161-223, 2000.

[4] A.P. Watkins and H. Khaleghi, Modelling diesel spray evaporation using a noniterative implicit solution scheme, *Applied Mathematical Modelling*, 14, 9, pp. 468-474, 1990.

[5] X.Q. Chen and J.C.F Perreira, Stochastic-probabilistic efficiency enhanced dispersion modelling of turbulent polydispersed sprays, Journal of Propulsion and Power, 12. pp. 760-769, 1996.

[6] J. Abraham, What is Adequate Resolution in the Numerical Computation of Transient Jets?, *SAE Paper No. 970051*, pp 141-145, 1997.

[7] V.A. Iyer and J. Abraham, Penetration and dispersion of transient gas jets and sprays, *Combustion Science and Technology*, 130, pp. 315-334, 1997.

[8] M. Hallmann, M. Scheurlen, and S. Wittig, Computation of turbulent evaporating sprays: Eulerian versus Lagrangian approach, *Journal of Engineering for Gas Turbines and Power*, 117, pp. 112-119, 1995.

[9] C. Krüger, Validierung eines 1d-Spraymodelles zur Simulation der Gemischbildung in direkteinspritzenden Dieselmotoren, Ph.D. thesis, RWTH Aachen, 2001.

[10] F.H. Harlow and A.A. Amsden, Numerical calculation of multiphase fluid flow, *Journal of Computational Physics*, 17, pp. 19-52, 1975.

[11] F.H. Harlow, Fluid dynamics in Group T-3 Los Alamos National Laboratory: (LAUR-03-3852), *Journal of Computational Physics*, 195, 2, pp. 414-433, 2004.

[12] V.A. Iyer, J. Abraham and V. Magi, Exploring injected droplet size effects on steady liquid penetration in a Diesel spray with a two-fluid model, *International Journal of Heat and Mass Transfer*, 45, pp. 519-531, 2002.

[13] R.I. Issa, P.J. Oliveira, Numerical prediction of phase separation in two-phase flows through T-junctions, *Comput. Fluids*, 23, pp. 347–372, 1994.

[14] A. Behzadi, R.I. Issa, H. Rusche, Modelling of dispersed bubble and droplet flow at high phase fractions, *Chemical Engineering Science*, 59, pp. 759-770, 2004.

[15] A.D. Gosman, C. Lekakou, S. Politis, R.I. Issa, M.K. Looney, Multidimensional modeling of turbulent two-phase flows in stirred vessels, *Aiche Journal*, 38, pp. 1946-1956, 1992.

[16] E. Riber, M. Moreau, O. Simonin, B. Cuenot, Development of Euler-Euler les approach for gas-particle turbulent jet flow, *Proceedings of ASME Fluids Engineering Division Summer Meeting*, pp. 1663-1672, 2006.

[17] D.A. Drew, S.L. Passman, Theory of Multicomponent Fluids, Springer, 1998.

[18] B. Abramzon, and W.A. Sirignano, Droplet Vaporization Model for Spray Combustion Calculations, *Int. J. Heat Mass Transfer*, pp. 1605-1618, 1989.

[19] G.M. Bianchi and P. Pelloni, Modeling the Diesel Fuel Spray Break-up by Using a Hybrid Model, *Proc. SAE 1999-01-0226*, pp. 27-42, 1999.

[20] R.D. Reitz, Modeling Atomization Processes in High-Pressure Vaporizing Sprays, *Atomization and Spray Technology*, 3, pp. 309-337, 1987.

[21] AVL List GmbH, Multiphase Flow, FIRE Version 8 user manual, Graz, Austria, 2008.

[22] E.v. Berg, A. Alajbegovic, R. Tatschl, C. Krueger, U. Michels, Multiphase Modelling of Diesel Sprays with the Eulerian/Eulerian Approach, *Proc. 17th Annual Conference on Liquid Atomisation and Spray Systems (ILASS-Europe '01)*, 2001.

[23] E.v. Berg, W. Edelbauer, A. Alajbegovic, R. Tatschl, Coupled Calculation of Cavitating Nozzle Flow, Primary Diesel Fuel Break-up and Spray Formation with an Eulerian Multi-fluid-model, *Proc. 9th International Conference on Liquid Atomisation and Spray Systems (ICLASS '03)*, CD-Proc. 12-02, 2003.

[24] E.v. Berg, W. Edelbauer, R. Tatschl, A. Alajbegovic, M. Volmajer, B. Kegl and L.C. Ganippa, Coupled Simulation of Nozzle Flow, Primary Fuel Jet Break-up, and Spray Formation, *Journal of Engineering for Gas Turbines and Power*, 127, pp. 897-908., 2005.

[25] M.A. Lopez de Bertodano, Two fluid model for two-phase turbulent jets, *Nuclear Engineering and Design* 179, pp. 65-74, 1998.

[26] J.Y. Chen, Joint Scalar PDF simulations of turbulent reacting flows with detailed chemistry on a parallel cluster, *3rd Intern. Workshop on measurement and Computation of Turbulent Non-premixed flames*, 1998.